Defect and Diffusion Forum
ISSN: 1662-9507, Vol. 429, pp 81-90
doi:10.4028/p-O0aFG5

Accepted: 2023-09-26
Online: 2023-12-12

CFD Analysis of Perforated Plates and Open-Cell Materials Aerodynamics

Antonio F. Miguel[1,2,*]

[1]Department of Physics, University of Évora, Portugal

[2]Institute of Earth Sciences, Pole of Évora, Portugal

[*]afm@uevora.pt

Keywords: perforated places, open-cell materials, fluid flow, dimensionless loss factor, permeability, Forchheimer coefficient, aerodynamics.

Abstract. In this paper, a numerical study of fluid flow through perforated panels with square holes and open-cell material with cubic cells is presented. Structures with a wide variety of porosities ($0.15<\varphi<0.94$) and Reynolds numbers ($0.01<Re<6000$) are studied. Among the various outcomes obtained, the results indicate that pressure gradient vs Reynolds number exhibits three different forms of variation, including linear ($Re<1$), nonlinear ($1\leq Re<4000$), and one where the pressure gradient is virtually constant with the Reynolds number ($Re\geq 4000$). The results were provided in terms of loss factor, but also of intrinsic permeability and the Forchheimer coefficient. Relationships that connect porosity to the loss factor, intrinsic permeability, and Forchheimer coefficient are also presented. These findings may prove useful in better understanding the flow behaviors in perforated panels and cell metal foams, which have a wide range of applications.

Introduction

Perforated plates have been employed in a variety of areas ranging from sound absorption [1] and shading [2], to heat exchangers [3] and airflow control [4]. Both experimental and numerical simulation studies are available in the literature [5-8]. Yavuzkurt and Catchen [9] conducted wind tunnel tests on seven perforated plates with different thicknesses and porosities to examine the correlation between pressure loss and air velocity. The pressure loss versus air velocity dependence of 28 perforated plates (porosities varying from 0.227 to 0.694) with various hole shapes was investigated by Allori et al. [5], in a wind tunnel, for Reynolds numbers ranging from 1200 to 20000. Özahi [10] also examined the impact of pressure drop at low Reynolds numbers on perforated plates with different porosities.

Numerical investigations have been conducted on perforated plates with various structural parameters [11], hole shapes [7], and working fluids [12]. Thinner perforated plates resulted in higher pressure drops for turbulent flow, according to Bayazit et al. [13], while thicker perforated plates caused higher pressure drops for laminar flow. In a wide range of porosity (0.15 to 0.90), Miguel [7] studied the performance of several perforated plate designs and showed that the flow resistance of perforated plates with noncircular holes is lower than that of perforated plates with circular holes.

Open-cell metal foams with macro-sized voids are frequently utilized in the aerospace industry and other engineering applications, as lightweight materials for heat transfer support structures, and as sound-absorbing materials [14-15]. They are characterized by high specific surface area, high porosity, and lightweight. These foams are unquestionably three-dimensional structures, and they deserve to be investigated. Some studies have concentrated on the study of flow permeability and heat conductivity as functions of porosity]16,17].

In this study, fluid flow through perforated panels and open-cell structures is examined numerically. The performance of these systems is investigated, and hydrodynamic characteristics such as the loss factor, the permeability to fluid flow, and the Forchheimer coefficient are obtained.

Model and Methodology

Perforated plates. In this work, perforated plates with square holes of various sizes are investigated. Each plate (0.200 m x 0.200 m x 0.01 m) is perforated with 9 evenly spaced holes (Fig. 1). The length of holes ranges from 0.026 m to 0.064 m, translating to a porosity range of 0.152 to 0.922.

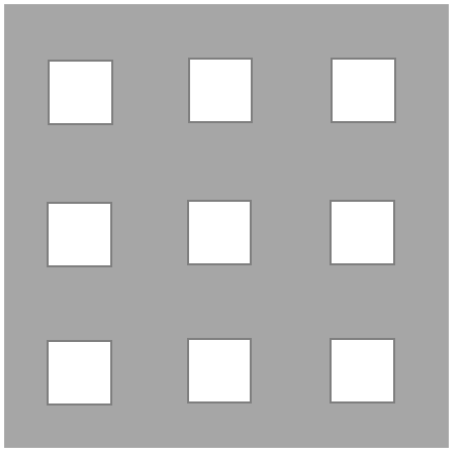

Fig. 1. A schematic of the proposed perforated plates with square holes.

Open-cell structures. This study also looks at arrangements of basic cubic unit cells, as seen in Fig. 2.

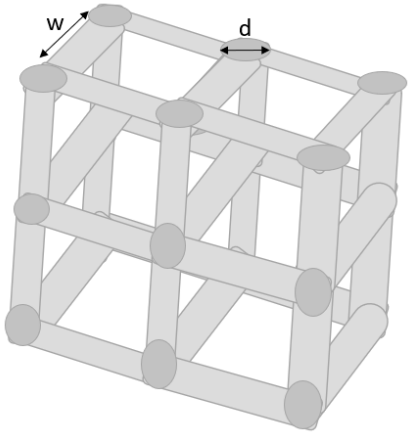

Fig. 2. A schematic of a cubic unit cell-based 3D configuration.

The configuration's solid portion is made up of cylindrical-shaped elements, and the porosity for the arrangement spans from 0.237 to 0.932, and it is obtained based on the length w and diameter d (Fig. 2), according to

$$\varphi = 1 - \frac{d^3}{w^3}\left(0.75\pi\frac{w}{d} - 2^{1/2}\right) \quad (1)$$

where φ is the porosity.

Governing Equations. A steady Reynolds averaged conservation equations are as follows:

Continuity equation

$$\frac{\partial V_i}{\partial x_i} = 0 \quad (2)$$

Momentum equation

$$\rho \frac{\partial (V_i V_j)}{\partial x_j} = -\frac{\partial p}{\partial x_i} + \frac{\partial}{\partial x_j}\left[\mu\left(\frac{\partial V_i}{\partial x_j} - \rho\overline{V_i' V_j'}\right)\right] \quad (3)$$

where V is the component of fluid velocity, V′ is a fluctuating component of velocity, ρ is the fluid density, μ is the dynamic viscosity, and p is the pressure.

The RNG k- ε model is derived from the momentum equation by applying the so-called renormalization group method. In this study, simulations were carried out utilizing the finite-volume-based Ansys Fluent code [18,19]. Simulations of fluid flow are carried out for configurations shown in Figs. 1 and 2, with Reynolds numbers ranging from 0.01 to 6000. At the inlet boundary of the computational domain, a constant mass flow rate is prescribed. Atmospheric pressure is considered at the outlet of the computational domain. No-slip boundary condition at the solid surfaces is employed. In order to discretize the governing equations, a second-order upwind approach is used. SIMPLE algorithm is employed to solve pressure-velocity coupling. Residual conditions are set to 10^{-5} and 10^{-9} for the continuity equation and momentum equations, respectively.

Unstructured grids are employed, and a mesh sensitivity analysis based on ASME criteria [20] for each configuration is conducted to examine the effect of grid resolution on results.

Results and Discussion

To validate the flow simulation, pressure gradients across perforated panels with square holes resulting from the numerical simulations are compared to Allori et al. [5,6] experimental data. Fig. 3 depicts the results for fluid flow through the perforated plate and shows a good agreement between our simulation results and the experimental data. Notice that the curve from the numerical simulations is within the experimental error bars.

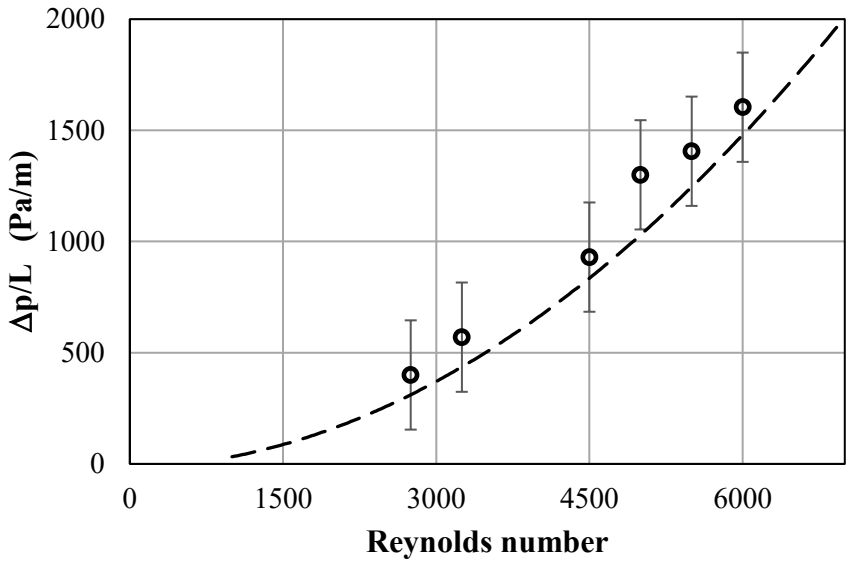

Fig. 3. Pressure gradient vs. Reynolds number through perforated panels: experimental data (φ=0.44) [5,6] and —— numerical prediction (φ=0.45).

We may now study several aspects of fluid flow through structures with void spaces using our numerical approach. In Fig. 4, pressure gradients for perforated plates (Fig. 1) are plotted against Reynolds numbers. As expected, this plot shows that the pressure gradient diminishes with increasing porosity. More significant is that it depicts three types of dependence between the pressure gradient and the Reynolds number: one where the pressure gradient varies linearly with the Reynolds number (Re<1), one where the pressure gradient variation with the Reynolds number variation is not linear

(1≤Re<4000), and one where the pressure gradient is almost constant with the Reynolds number (Re≥4000).

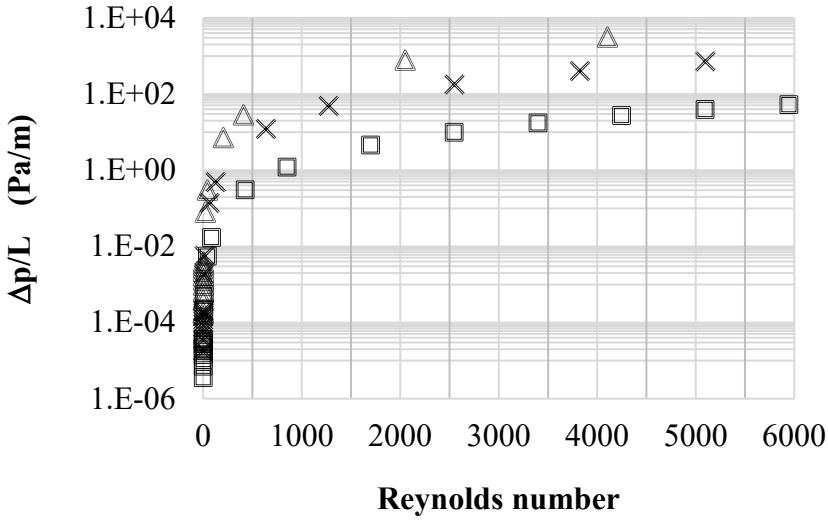

Fig. 3. Pressure gradient vs. Reynolds number through perforated panels: φ=0.3 (Δ); φ=0.6 (x); φ=0.9 (□).

The loss factor, which depends on both system's geometry and the flow regime, is a crucial dimensionless parameter defined by the ratio of pressure drop to the product of the density and the square of average flow velocity. The loss factor for the three variation intervals identified in Fig. 3 is shown in Figs. 4 to 6.

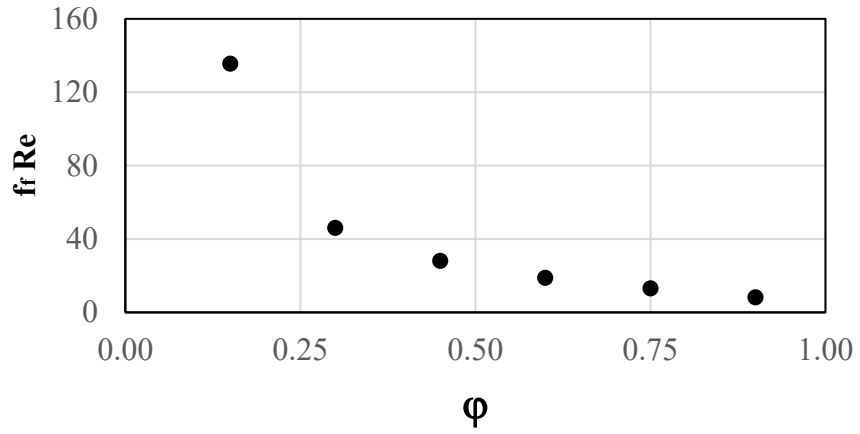

Fig. 4. The product of the loss factor by the Reynolds number vs the porosity (Re<1).

The results shown in Figs. 4 to 6 can be fitted using the subsequent set of equations:

$$f_r = \frac{7.991}{Re\ \varphi^{1.5}} \quad r^2=0.999 \quad (Re<1) \tag{4}$$

$$f_r = \frac{89.2}{\ln(Re)^{0.25}\exp(3.886\varphi)} \quad r^2=0.982 \quad (1\leq Re<4000) \tag{5}$$

$$f_r = \frac{257.33}{\exp(7.968\varphi)} \quad r^2=0.990 \quad (4000\leq Re<6000) \tag{6}$$

where f_r is the loss factor and φ is the porosity. For Re<1, the loss factor drops as porosity is raised to power 1.5, while for Re≥ 1 the loss factor exhibits a negative exponential relationship with the porosity. As anticipated, for Re>4000 the loss factor is not dependent on the Reynolds number.

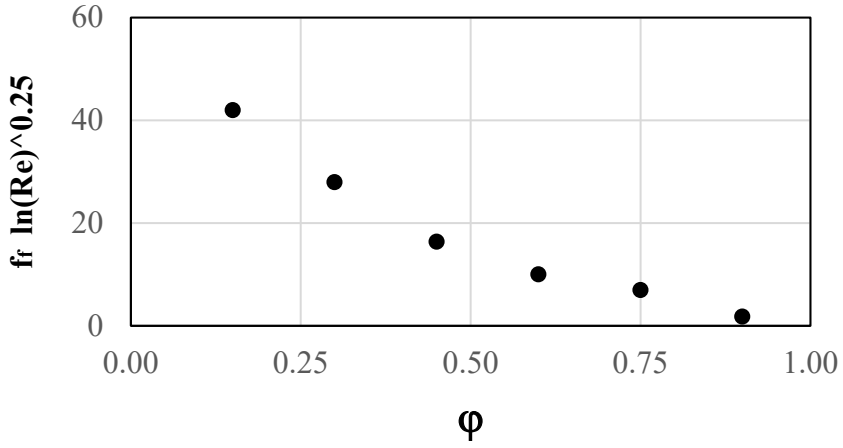

Fig. 5. The product of the loss factor by $\ln(Re)^{0.25}$ vs the porosity 1≤Re<4000).

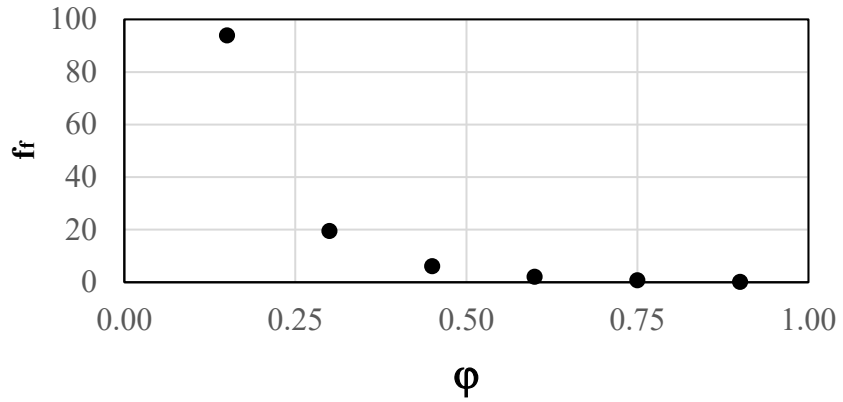

Fig. 6. Loss factor vs the porosity (4000< Re ≤6000).

The analysis frequently employed for porous materials can also be used. Darcy's law defines there is a linear relationship between flow velocity and pressure gradient, in a permeable media under creeping-flow conditions. When this linear relationship between pressure gradient and velocity is no longer adequate to explain the fluid flow, the Darcy-Forchheimer equation can be used to account for these nonlinear effects [21,22]

$$\frac{\Delta p}{L} = \frac{\mu}{K} u + \frac{\rho \lambda}{K^{1/2}} u^2 \tag{7}$$

Here λ is a dimensionless parameter for the non-linear velocity term (the Forchheimer coefficient), μ is the fluid dynamic viscosity, K is the intrinsic permeability of the perforated panel, u is fluid velocity and L is the thickness of the panel.

To calculate the intrinsic permeability and the Forchheimer coefficient, the pressure gradient versus fluid velocity data is fitted to the Darcy-Forchheimer equation. The outcomes are shown in Figs. 7 and 8. According to these figures, the intrinsic permeability rises with porosity whereas the inertial coefficient rises as porosity decreases.

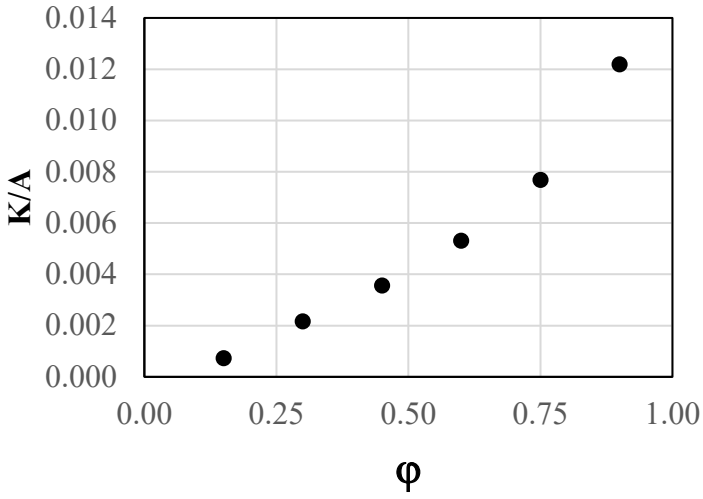

Fig. 7. The ratio of intrinsic permeability to the area of one square hole vs the porosity.

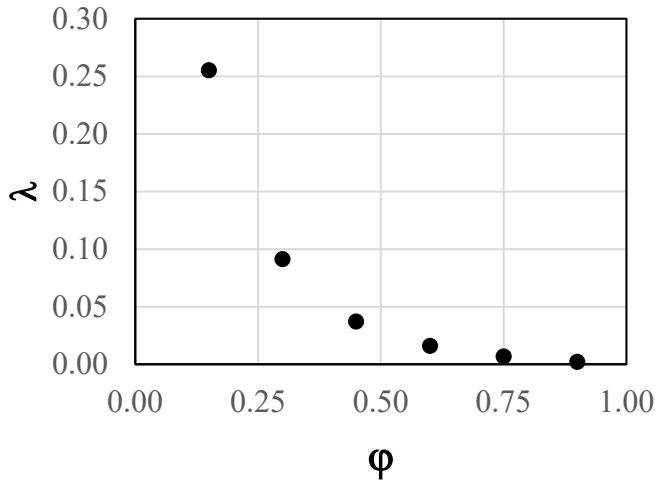

Fig. 8. The Forchheimer coefficient vs the porosity.

The data set shown in Figs. 7 and 8 are best described by the following equations

$$\frac{K}{A} = 0.0125\varphi^{1.5} \qquad r^2=0.975 \tag{8}$$

$$\lambda = \frac{0.6353}{\exp(6.234\varphi)} \qquad r^2=0.999 \tag{9}$$

These findings demonstrate that the Kozeny-Carman equation [7,21] is inadequate to explain our numerical results for perforated panels. Furthermore, Eqs. (8) and (9) are consistent with those presented in other studies for high porosity media (e.g., Koponen et al. [23], Miguel et al. [24]). It is also worth noting that the dependence found between the Forchheimer coefficient and porosity corresponds with prior findings [7,23].

For a cubic unit cell-based structure (Fig. 2), the pressure gradient computed numerically versus the Reynolds number is illustrated in Fig. 9. Similar to what happened with the perforated panels, there is a clear change from linear (creeping flow) to nonlinear flow at Re~1.

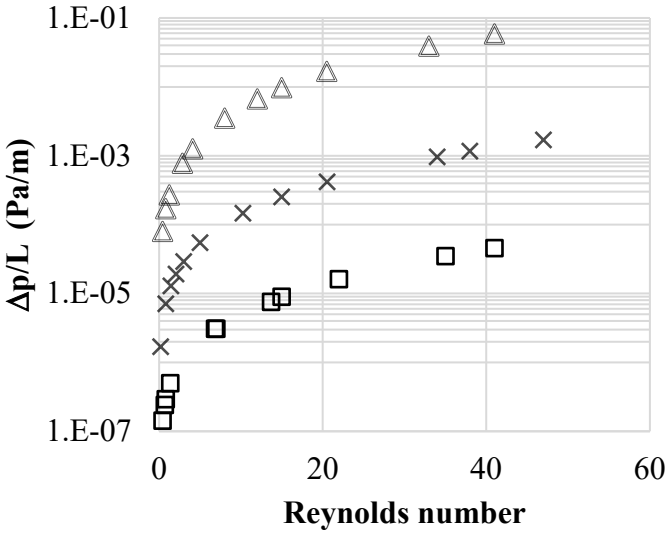

Fig. 9. Pressure gradient vs. Reynolds number through cubic unit cell-based configuration: φ =0.3 (Δ); φ =0.6 (x); φ =0.9 (□).

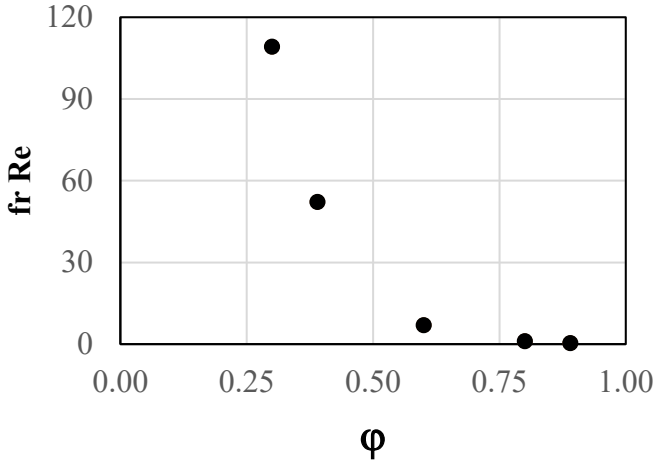

Fig. 10. The product of the loss factor by the Reynolds number vs the porosity (Re<1).

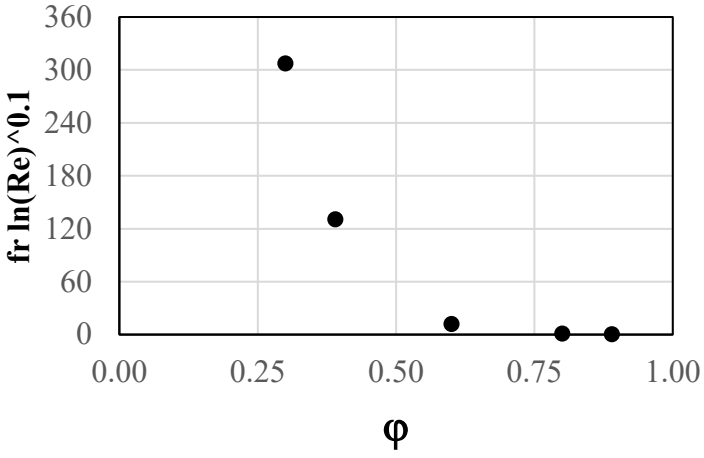

Fig. 11. The product of the loss factor by $\ln(Re)^{0.1}$ vs the porosity $1 \leq Re < 60$)

Next, the loss factor for a structure based on cubic unit cells is investigated. Both porosity and Reynolds number have an impact on the loss factor, as seen in Figs. 10 and 11. The equations that fit the data set in these figures are

$$f_r = \frac{0.2977}{Re\ \varphi^{5.215}} \quad r^2=0.950 \quad (Re<1) \tag{10}$$

$$f_r = \frac{9124}{\ln(Re)^{0.1}\exp(11.07\varphi)} \quad r^2=0.997 \quad (1\leq Re<60) \tag{11}$$

It should be noticed that the generic equations for the loss factor that describe the general dependence on porosity and Reynolds number produced by the perforated plate and cubic unit cell-based configuration are the same.

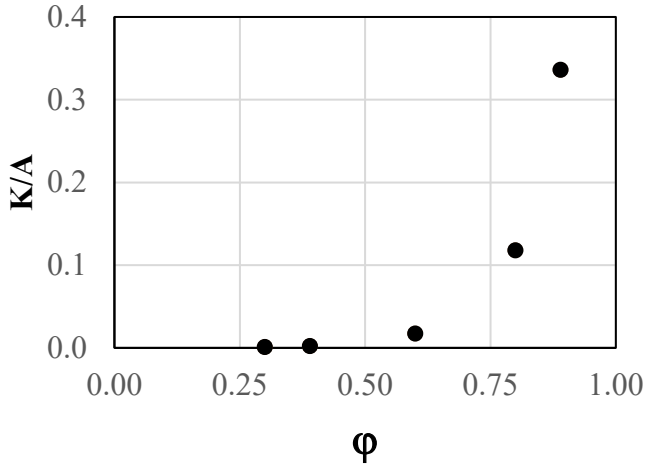

Fig. 12. The ratio of intrinsic permeability to the area of one unit cell vs the porosity

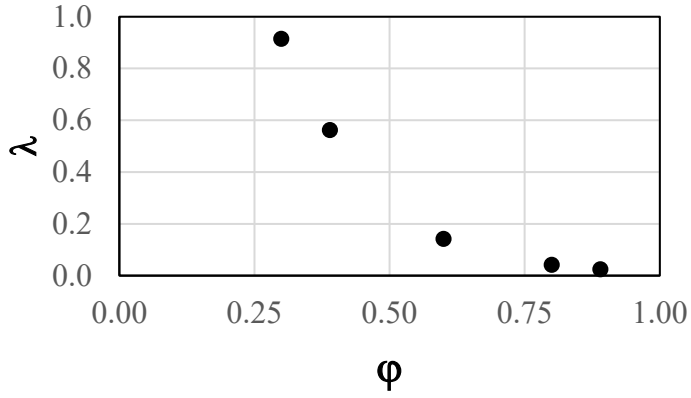

Fig. 13. The Forchheimer coefficient vs the porosity

Figs. 12 and 13 show the intrinsic permeability and Forchheimer coefficient of a cubic unit cell-based structure as a function of its porosity. As for perforated plates, permeability increases with porosity, although the Forchheimer coefficient decreases with porosity. The data displayed in these figures are best fit by the ensuing equations

$$\frac{K}{A} = 0.4031\varphi^{5.215} \quad r^2=0.952 \tag{12}$$

$$\lambda = \frac{6.1055}{\exp(6.24\varphi)} \quad r^2=0.998 \tag{13}$$

These findings show that the Kozeny-Carman equation is equally inappropriate for both the cubic unit cell-based structure and perforated plates. To add, it should be noted that the outcomes are consistent with findings for the relationship between intrinsic permeability and porosity [23,24] as well as studies for the correlation between the Forchheimer coefficient and porosity reported by [7,23].

Conclusion

This study examines how structure affects the loss factor, permeability, and Forchheimer coefficient. Perforated panels with square holes and open-cell materials with cubic cells serve as representations of solid materials with voids. A numerical study of fluid flow through these structures that spans a large range of porosity ($0.15<\varphi<0.94$), as well as Reynolds number ($0.01<Re<6000$) is performed. The results are used to compute the geometry's loss factor, permeability, and inertial coefficient. The findings show that porosity affects the loss factor, permeability, and Forchheimer coefficient. Also offered are new equations for the loss factor, permeability, and inertial coefficient. The sort of dependence on porosity for the loss factor depends on the Reynolds number range that is taken into account. The Forchheimer factor is connected to the exponential porosity, while permeability is related to porosity increased to a power.

References

[1] D. Li, D. Chang, B. Liu, Appl. Acoust. 127 (2017) 316–323.

[2] A.F. Miguel, A. Silva, Applied Energy 87 (2010) 836-842.

[3] V. Babak, T. Babak, L. Kholpanov, V.A. Malyusov, J. Eng. Phys. 50 (1986) 330–335.

[4] R. Liu, D. Ting, J. Fluids Eng. ASME 129 (2007) 1164–1171.

[5] D. Allori, G. Bartoli, A. F. Miguel, Int. J. Fluid Mech. Res. 39 (2012) 136–148.

[6] D. Allori, G. Bartoli, A. F. Miguel, 7th International Conference on Diffusion in Solids and Liquids (2011), 127.

[7] A.F. Miguel, Journal of Porous Media 22 (2019)1439–1448.

[8] Y. Bayazit, E. M. Sparrow, D. D. Joseph, Int. J. Therm. Sci. 85 (2014) 104–111.

[9] S. Yavuzkurt, G. L. Catchen, ASME International Mechanical Engineering Congress and Exposition 37165 (2003) 435–440.

[10] E. Özahi, Flow Meas. Instrum. 43 (2015) 6–13.

[11] Y. Bae, Y.I. Kim, Chem. Eng. Sci. 149 (2016) 78–87.

[12] A.L. Teh, K.W. Chin, E.K. Teh, W.M. Chin, C.M. Chia, J.J. Foo, Chem. Eng. Res. Des. 100 (2015) 57–71.

[13] Y. Bayazit, E.M. Sparrow, D.D. Joseph, Int. J. Therm. Sci. 85 (2014) 104–111.

[14] H.F. Abbasov, Int. J. Thermophys. 41 (2020) 164.

[15] L. Li, B. Han, S. Y. He, Z. Y. Zhao, R. Zhang, Q. C. Zhang, T. J. Lu, Mater. Des. 164 (2019) 107546.

[16] A.H. Khalid, M. H. Ismail, H. B. A. Kasim, H. F. Pahroraji, M. A. B. Zainol, A. M. M. B. M. Azaiauddin, IOP Conf. Ser.: Mater. Sci. Eng. 834 (2020) 012029.

[17] H. Yang, Y. Li, B. Ma, Y. Zhu, Materials 14 (2021) 3153.

[18] ANSYS FLUENT 16.2, User's Guide. www.fluent.com.

[19] M.B. Acikgoz, B. Akay, A.F. Miguel, M. Aydin, Defect and Diffusion Forum 312-315 (2011) 865-870.

[20] I.B. Celik, U. Ghia, P.J. Roache, C.J. Freitas, H. Coleman, P.E. Raad, J. Fluids Eng. 130 (2008) 078001.

[21] A. F. Miguel, Thermal Science 16 (2012) 167-176.

[22] A. Koponen, D. Kandhai, E. Hellen, Phys. Rev. Lett. 80 (1998) 716.

[23] A. F. Miguel, Energy and Buildings 28 (1998) 63-69.